



# Tsunami Vulnerability and Risk Analysis Applied to the City of Alexandria, Egypt

Róbert Jelínek, Sandra Eckert, Gunter Zeug and Elisabeth Krausmann



EUR 23967 EN - 2009



# Tsunami Vulnerability and Risk Analysis Applied to the City of Alexandria, Egypt

Róbert Jelínek, Sandra Eckert, Gunter Zeug and Elisabeth Krausmann

EUR 23967 EN - 2009



The mission of the Institute for the Protection and Security of the Citizen is to provide research results and to support EU policy-makers in their effort towards global security and towards protection of European citizens from accidents, deliberate attacks, fraud and illegal actions against EU policies.

European Commission  
Joint Research Centre  
Institute for the Protection and Security of the Citizen

The drawing on the front cover illustrates the Lighthouse of Alexandria (Pharos) by German archaeologist Prof. H. Thiersch (1909). The Lighthouse was damaged by several earthquakes, (source: <http://en.wikipedia.org> en.wikipedi)

**Contact information**

Address: Via E. Fermi 2749, 210 27 Ispra, Italy  
E-mail: [robert.jelinek@jrc.it](mailto:robert.jelinek@jrc.it)  
Tel.: +39 0332 78 9297  
Fax: +39 0332 78 9007

<http://ipsc.jrc.ec.europa.eu>  
<http://www.jrc.ec.europa.eu>

**Legal Notice**

Neither the European Commission nor any person acting on behalf of the Commission is responsible for the use which might be made of this publication.

A great deal of additional information on the European Union is available on the Internet.

It can be accessed through the Europa server  
<http://europa.eu/>

JRC53316

EUR 23967 EN  
ISSN 1018-5593

Luxembourg: Office for Official Publications of the European Communities

© European Communities, 2009

Reproduction is authorised provided the source is acknowledged

*Printed in Italy*

## Table of contents

|  |    |
|--|----|
| Table of contents.....   | ii |
| List of tables and figures.....  | iv |
| ABSTRACT.....  | 6  |
| 1. INTRODUCTION .....  | 8  |
| 2. DESCRIPTION OF THE INVESTIGATED AREA.....                                       | 10 |
| 3. HAZARD ANALYSIS .....   | 11 |
| 3.1. Methodological Background.....  | 11 |
| 3.2. Results of the Analysis.....  | 15 |
| 4. VULNERABILITY ANALYSIS.....   | 18 |
| 4.1. Introduction.....   | 18 |
| 4.2. Field Data Collection .....   | 19 |
| 4.3. Satellite Data, Processing and Resulting Products .....                       | 22 |
| 4.4. Vulnerability Parameters Derived from Generated Remote Sensing Products ..... | 26 |
| 4.5. Physical Vulnerability Results.....   | 28 |
| 5. RISK ANALYSIS.....  | 30 |
| 5.1. Methodological Background.....  | 30 |
| 5.2. Tsunami Risk Results .....  | 32 |
| 6. DISCUSSION AND CONCLUSIONS .....  | 36 |
| REFERENCES .....   | 39 |



## List of tables and figures

|  |    |
|--|----|
| Table 1: Tsunami hazard zones for Australia and its island territories.....  | 13 |
| Table 2: Tsunami hazard severity degree with respect to wave height and ground elevation...  | 13 |
| Table 3: Tsunami water height categories .....   | 14 |
| Table 4: Relation between verbal descriptor and indicative value of probability .....  | 14 |
| Table 5: Acquisition angles of the stereo IKONOS dataset .....   | 22 |
| Table 6: Point residual statistics achieved after rational polynomial optimization .....   | 23 |
| Table 7: Accuracy assessment of the derived DEM, building height and number of floors layer .....  | 25 |
| Table 8: Selected parameters for the physical vulnerability calculation and class allocation scheme.....   | 26 |
| Table 10: Distribution of building types in the investigated areas .....   | 36 |
|  |    |
| Figure 1: Epicentral distribution of instrumental earthquakes recorded in the lower Nile delta between 1900 and 1997 together with major active fault trends .....   | 8  |
| Figure 2: Overview of the two study sites in Alexandria; El Gomrok (left square) and El Montazah (right square). Red stars indicate the distribution of the differential GPS measurements collected during the field mission .....   | 11 |
| Figure 3: The tsunamigenic zones of the Mediterranean Sea .....  | 12 |
| Figure 4: The building water height distribution maps for the 5 and 9 m scenario in: a) El Gomrok area and b) El Montazah area, Alexandria .....   | 17 |
| Figure 5: Overview of the building type data collected in the two study sites (green stars).....   | 20 |
| Figure 6: Building types found in El Gomrok and El Montazah. Examples for a neglected building (upper left), a traditional brick building (upper right), a well maintained old building along the Corniche (lower left), a modern, tall building in El Montazah (lower right)..... | 21 |
| Figure 7: Quicklook of the acquired IKONOS stereo dataset .....  | 22 |
| Figure 8: Generated DSM for the two study sites, black areas represent no data areas or failed matching areas .....  | 24 |
| Figure 9: Derived DEM for both study sites.....  | 24 |
| Figure 10: Average elevation at every building polygon centroid .....  | 27 |
| Figure 11: Calculated number of floors for every building polygon .....  | 27 |
| Figure 12: Building type layer collected by visual examination in Alexandria .....   | 28 |

Figure 13: Physical vulnerability map for the study site El Gomrok ..... 29

Figure 14: Physical vulnerability map for study site El Montazah..... 30

Figure 15: Tsunami building risk zonation maps in El Gomrok area for: a) 5 m scenario and b) 9 m scenario ..... 33

Figure 16: The pair column chart of tsunami building risk for the 5 m event (in blue) and the 9 m scenario (red stripes)..... 33

Figure 17: Tsunami building risk zonation maps in El Montazah area for: a) 5 m scenario and b) 9 m scenario..... 35

Figure 18: Chart showing distribution of tsunami risk in El Montazah area for 5 (in blue) and 9 m (red stripes) scenarios ..... 35

## ABSTRACT

Even though tsunamis are relatively rare in the Mediterranean Sea, their potential risk cannot be neglected. Alexandria was not affected by a major earthquake or tsunami in recent years. However historical events show that approximately 5,000 people lost their lives and 50,000 homes were destroyed in the city after the earthquake in 365. The Roman historian Ammianus Marcellinus wrote about the impact of this event in Alexandria: *The solidity of the whole earth was made to shake and shudder, and the sea was driven away. The huge mass of waters returning when least expected killed many thousands by drowning. Huge ships perched on the roofs of houses and others were hurled nearly 3 kilometers from the shore*". The last tsunami to hit the eastern Mediterranean occurred on August 8, 1303. It destroyed the great lighthouse of Alexandria, one of the seven wonders of the ancient world. In order to avoid such events in the future, a detailed knowledge about the tsunami phenomenon and its potential consequences is needed.

In this study very high resolution satellite remote sensing data have been used to calculate the tsunami hazard, the physical vulnerability and risk for a central and peri-urban district of the city of Alexandria. The central study site is located in the historic old town of Alexandria, which is a part of El Gomrok district. The peri-urban study site is situated in the northeast of Alexandria, bordering Montazah Palace and covering a part of El Montazah district.

Tsunami hazard analysis focuses on the description of both the tsunami severity and its frequency in order to create tsunami hazard maps. A tsunami is generally described by the tsunamigenic sources and their characteristics needed for propagation and inundation modeling. Since numerical models for propagation and inundation were not applied to this site, we used the water height, or depth of inundation, obtained by a so-called "bathtub" approach to characterize the tsunami hazard. The water height was divided into five categories: very low, low, medium, high and very high. Based on historical records of past tsunamis, two inundation scenarios of 5 m and 9 m run-up height were assumed to perform the physical vulnerability and risk analysis. The physical vulnerability assessment was performed by the ISFEREA group of the JRC. The vulnerability results presented in this study are based on a conference paper prepared by Eckert and Zeug, 2009. According to

their methodology, the building vulnerability is based on the four indicators: elevation, building type, number of floors and shoreline distance. These indicators were derived from stereo remote sensing data in combination with a field survey.

Once the hazard and vulnerability components were known, the next step was to estimate risk. This was performed by the MAHB group of the JRC. Tsunami risk can be expressed and measured in a variety of ways and there is no unique definition of risk. In the proposed study, tsunami risk is expressed as a product of hazard times vulnerability. Risk can be usually estimated for people (e.g. in terms of people loss or injuries) or property (e.g. loss of value of property). Since the vulnerability analysis was carried out for buildings, the same was done for the risk. This has been done in a qualitative way using a risk matrix of 5x5 classes, which relates the hazard and vulnerability. The resultant building tsunami risk maps are categorized into the five risk levels very low, low, medium, high and very high.

The information obtained in this study can help the competent authorities to reduce potential tsunami consequences based on the resultant tsunami building vulnerability and risk maps.

## 1. INTRODUCTION

The situation about the awareness of tsunami risk in the Mediterranean region can be illustrated by a statement from Papadopoulos and Fokaefs, 2005 according to which it was a widely held believe that tsunamis either did not occur in the Mediterranean Sea or they were so rare that they did not pose a treat to coastal communities. Even though tsunamis are relatively rare in the Mediterranean Sea, their potential risk cannot be neglected because of their destructive power. The city of Alexandria was not affected by a major earthquake or tsunami in recent years. Highly destructive tsunamis were recorded at a number of locations in the Mediterranean but only few events are known that had affected Alexandria on the north coast of Egypt. Nevertheless, various earthquake events are documented for the Egyptian coast making Alexandria a hazardous place as two fault lines, the Suez-Cairo-Alexandria Line and Qattara-Eratosthenes Line, converge in the area (see Figure 1).

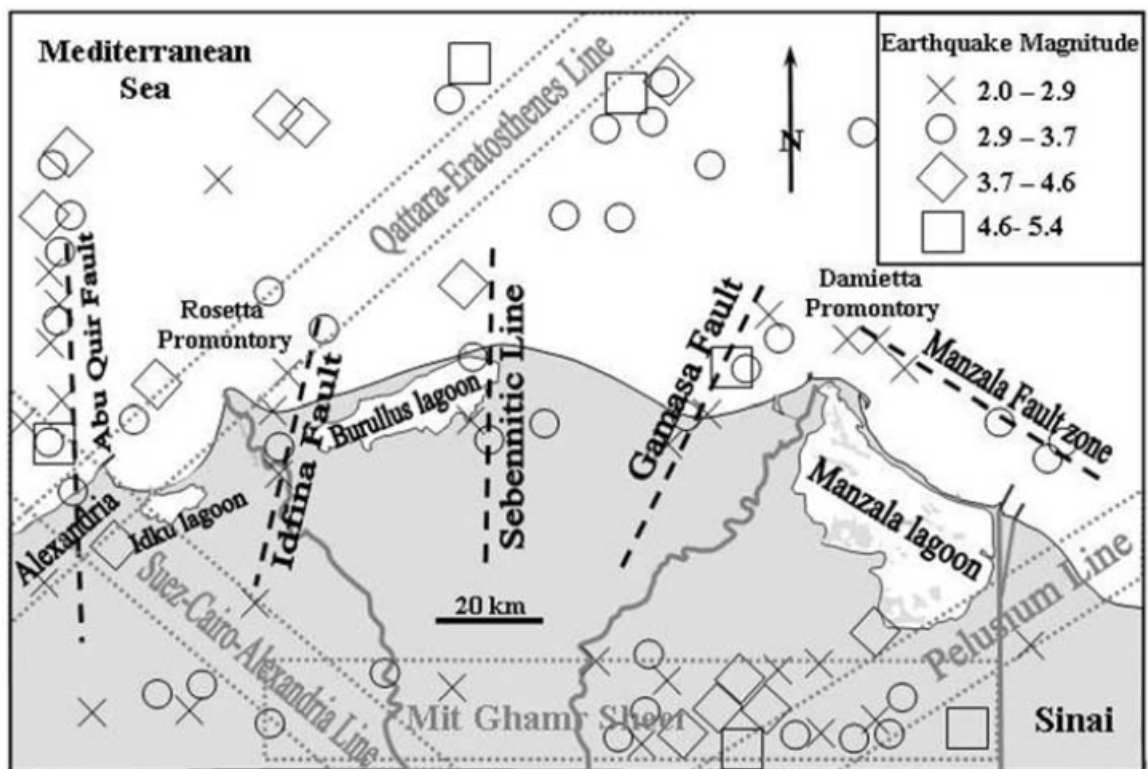


**Figure 1: Epicentral distribution of instrumental earthquakes recorded in the lower Nile delta between 1900 and 1997 together with major active fault trends (Frihy, 2003)**

Two strong tsunamigenic earthquakes that devastated the city of Alexandria are well known from historical records. Approximately 5,000 people lost their lives and 50,000 homes were destroyed after a powerful earthquake off the coast of Greece in 365. The tsunami that developed because of the quake destroyed the complete coastal regions as far as Egypt and eastern Sicily. In 1303 another earthquake destroying Rhodes caused a tsunami which reached the Egyptian coast. In Alexandria, many houses were ruined and much of the city wall was destroyed: 46 buttresses and 17 towers collapsed killing a large number of people. The lighthouse at Alexandria, which was one of the seven wonders of the ancient world, was shattered and its top collapsed (El-Sayed et al. 2000).

The 2004 Indian Ocean tsunami has reminded us that tsunamis may have a significant impact on a number of coastal areas in the world and can affect thousands of people. Since then efforts increased to understand the mechanisms of tsunami generation, propagation and coastal run-up and to implement operationally working early warning systems. For the Mediterranean an early warning system is currently being implemented that is providing warning on several hierarchy levels: local warning units at the very local level (e.g. municipality, district), regional warning units at an intermediate level (province, region, nation), and a global warning system at the higher level covering the whole Mediterranean (Boschi et al., 2005). The implementation of an early warning system requires also creating awareness of tsunami risk among the people in the vulnerable coastal areas. Thus, vulnerable areas have to be identified and the potential risk of a tsunami has to be assessed. This is essential for effective disaster planning as sensible mitigative measures cannot be developed fully or implemented effectively until a meaningful analysis has been undertaken. Population and infrastructure within any given tsunami flood zone are not uniformly at risk. This is because risk (the probability for damage) is intimately related to vulnerability (Alexander, 2000).

This report describes the work carried out by two research groups at the European Commission's Joint Research Centre (JRC), ISFEREA<sup>1</sup> and MAHB<sup>2</sup>, to achieve the project objectives of Work Package 8.7 of the 6<sup>th</sup> Framework Programme TRANSFER project, which was to produce tsunami risk-related products for the town of Alexandria. Deliverable D8.8 of the TRANSFER project specifies the production of flooding maps,

---

<sup>1</sup> ISFEREA- Geo-Spatial Information Analysis for Global Security and Stability

<sup>2</sup> MAHB- Major Accident Hazard Bureau

vulnerability maps with selected indicators and scenario risk maps. Since the flooding maps were not available when performing the analyses, we had to characterize the tsunami hazard by a single parameter, which was a water height recorded on each building using a bathtub approach. The vulnerability analysis focused on the building environment (physical vulnerability). The analysis of the population vulnerability, which was carried out by the UNU-EHS is discussed separately (UNU-EHS, 2009). The parameters describing the physical vulnerability were derived from stereo remote sensing data and a field survey. The tsunami risk was calculated using a risk matrix relating the hazard and vulnerability.

This report is divided into six chapters. After the Introduction, the study area is briefly described in Chapter 2. Chapters 3, 4 and 5 are dedicated to the hazard, vulnerability and risk analysis. Each of these chapters includes the methodological background and the results of the analyses. Discussions and conclusions from the study are summarized in a final chapter of the report.

## 2. DESCRIPTION OF THE INVESTIGATED AREA

Alexandria, known as "The Pearl of the Mediterranean" is the second largest city in Egypt. The city extends about 32 km along the coast of the Mediterranean Sea in north-central Egypt. The analyses in this study were performed in a central and a peri-urban part of the city of Alexandria (Figure 2). The central part is located in the historic old town of Alexandria, which is in El Gomrok district. The peri-urban study site is situated in the northeast of Alexandria, bordering Montazah Palace and covering a part of El Montazah district.

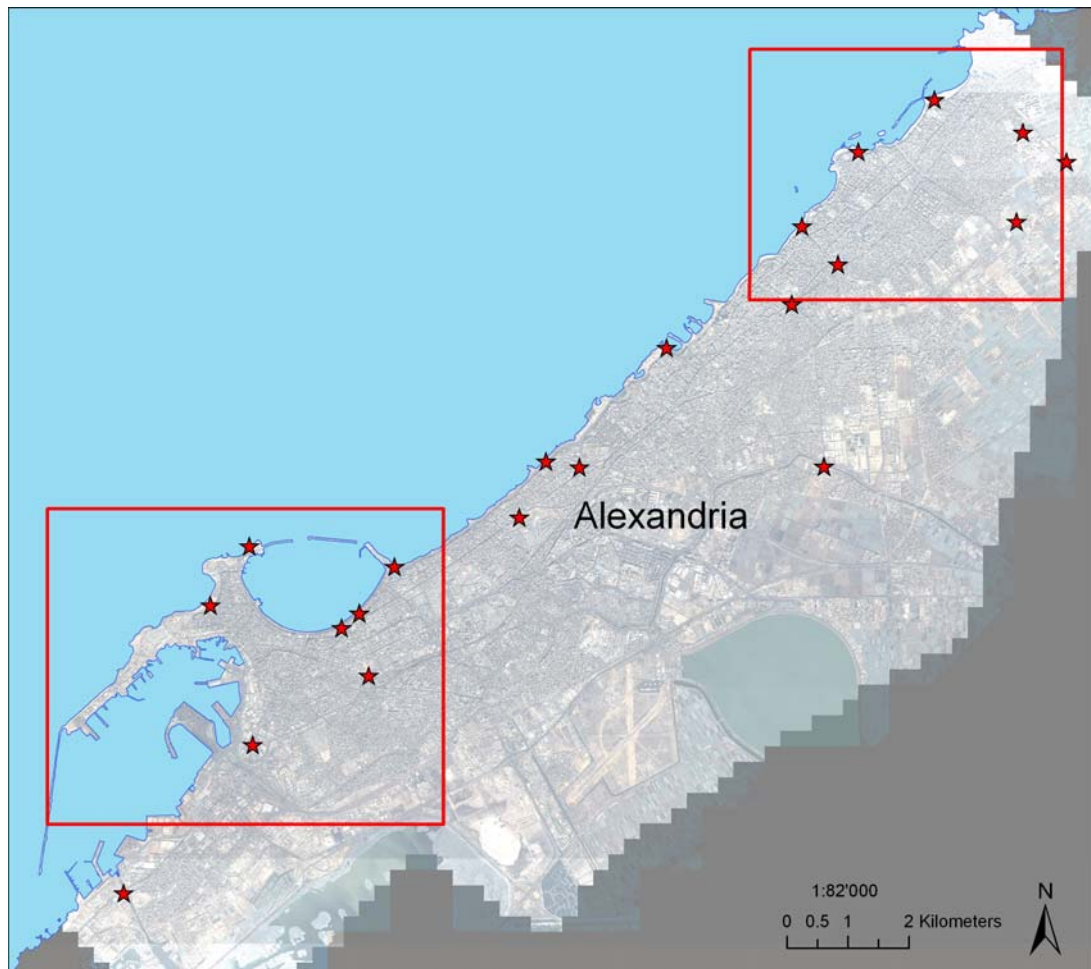


**Figure 2: Overview of the two study sites in Alexandria; El Gomrok (left square) and El Montazah (right square). Red stars indicate the distribution of the differential GPS measurements collected during the field mission**

### 3. HAZARD ANALYSIS

#### 3.1. Methodological Background

Tsunami hazard analysis focuses on both the tsunami severity and its frequency in order to create tsunami hazard maps. A tsunami is described by the tsunamigenic sources and their general characteristics needed for propagation and inundation modelling. The frequency describes the number of occurrences of a repeating tsunami event per unit time.

Tsunamigenic sources for the Mediterranean region are usually associated with earthquakes, volcanic eruptions and landslides in the Mediterranean basin (Papadopoulos and Fokaefs, 2005). A map of the known tsunamigenic sources in the Mediterranean Sea is illustrated in Figure 3.

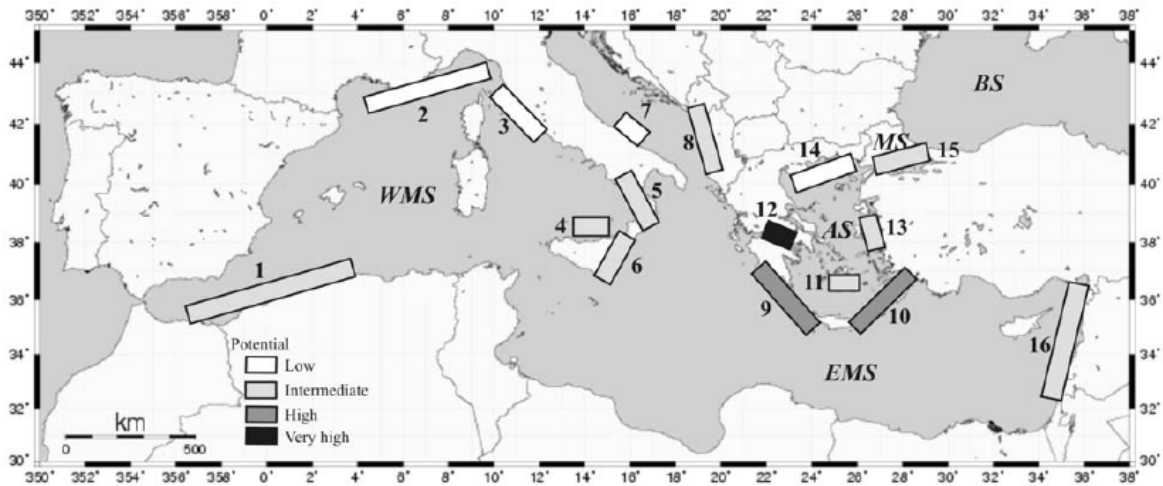


**Figure 3: The tsunamigenic zones of the Mediterranean Sea: WMS= West Mediterranean Sea, EMS= East Mediterranean Sea, AS = Aegean Sea, MS= Marmara Sea, BS= Black Sea, 1= Alboran Sea, 2= Liguria and Cote d’ Azur, 3= Tuscany, 4= Calabria, 5= Aeolian islands, 6= Messina straits, 7= Gargano promontory, 8= South-East Adriatic Sea, 9= West Hellenic arc, 10= East Hellenic arc, 11 = Cyclades, 12 = Corinth Gulf, 13= East Aegean Sea, 14= North Aegean Sea, 15= Marmara Sea, 16= Levantine Sea (Papadopoulos and Fokaefs, 2005)**

The majority of tsunamis that affected Alexandria has its sources in the West and East Hellenic arcs, which are located about 500 km from the Egyptian coasts.

Since numerical models for wave propagation and inundation were not applied to this site, a so-called “bathtub” approach was used to characterize the tsunami hazard. In this approach the area is overlapped with a selected inundation scenario in order to obtain the maximum water height recorded at each building. A similar approach was used in the Gulf of Corinth, Greece, to estimate the vulnerability towards a hypothetical tsunami with a wave run-up of 5 m (Papathoma and Dominey-Howes, 2003). Another example can be found in Curtis and Pelinovsky (1999), where the authors suggest that population and facilities located below 15 m elevation above sea level can be considered for a preliminary estimation of the tsunami risk for the Pacific region.

A variety of parameters exists that control a tsunami and can be taken into account for the hazard characterization. These include run-up height, wave height, ground elevation, tsunami magnitude, intensity and distance from the source. Characteristics used to quantify tsunami hazard zones in Australia (Rynn and Davidson, 1999) are summarized in Table 1.

**Table 1: Tsunami hazard zones for Australia and its island territories (Rynn and Davidson, 1999)**

| Characteristics                                     | Tsunami hazard zones |           |          |
|---|----------------------|-----------|----------|
|   | High                 | Medium    | Low      |
| Run-up height                                       | > 4 m                | 2 -4 m    | < 2 m    |
| Tsunami magnitude                                   | > 2                  | 1         | < 0      |
| Tsunami wave height                                 | > 1 m                | 0.1 – 1 m | < 0.1 m  |
| Damage observed from historic tsunamis              | Significant          | Minor     | None     |
| Coastal adjacent to near-field tsunamigenic sources | Yes                  | No        | No       |
| Potential tsunami inundation in future              | Probable             | Possible  | Unlikely |

Another example can be found in Papadopoulus and Dermentzopoulus (1998). The authors considered the wave surge height and ground elevation range for 4 classes of tsunami hazard severity degree. Papathoma and Dominey-Howes (2003) selected only the ground elevation to classify 4 inundation depth zones, as illustrated in Table 2.

**Table 2: Tsunami hazard severity degree with respect to wave height and ground elevation**

| Papadopoulus and Dermentzopoulus 1998 |                       |                            | Papathoma and Dominey-Howes 2003 |                            |
|---------------------------------------|-----------------------|----------------------------|----------------------------------|----------------------------|
| Tsunami Hazard Severity Degree        | Wave Surge Height (m) | Ground Elevation Range (m) | Inundation depth zones (IDZ)     | Ground Elevation Range (m) |
| 1                                     | 0                     | 6-8                        | Very low                         | 4-5                        |
| 2                                     | 0-2                   | 4-6                        | Low                              | 3-4                        |
| 3                                     | 2-4                   | 2-4                        | Medium                           | 2-3                        |
| 4                                     | 4-6                   | 0-2                        | High                             | <2                         |

To characterize the tsunami hazard for the Alexandria site, we used the water height, or depth of inundation, obtained by the bathtub approach. It was difficult to classify the tsunami hazard zonation using only the water height, because this parameter alone does not tell much about the potential damage to buildings, or people instability, and it is therefore commonly used in a combination with a current velocity. However, as it was mentioned before, numerical models were not applied to this site, therefore the current velocity parameter was not available. In order to have at least a rough idea about the impact of the water height on buildings, we have used the flash-flood magnitude scale developed within the European PREVIEW project, which links the water height to potential consequences (PREVIEW, 2005). According to this scale the potential damage to buildings caused by a flash flood is “limited” for a water height of up to 0.5 m, while for a water height from 1 to 2 m the destruction of reinforced concrete buildings (walls, foundations) can be expected. The water height was divided into five categories: very low, low, medium, high and very high, as illustrated in Table 3.

**Table 3: Tsunami water height categories**

| Water height [m] | Assign category | Descriptor  |
|------------------|-----------------|---|
| 0-0.5            | 1               | Very low hazard<br>*Expected damage to buildings is limited   |
| 0.5-1.0          | 2               | Low hazard<br>*Destruction of non-shock-resistant buildings (wood, prefabricated, no foundation); damage to reinforced concrete buildings |
| 1.0-1.5          | 3               | Medium hazard, danger for most<br>*Destruction of reinforced concrete buildings (walls, foundations)                                      |
| 1.5-2.0          | 4               | High hazard   |
| >2.0             | 5               | Very high hazard, dangerous for all   |

\* Indicative information based on the flash flood magnitude scale (PREVIEW, 2005)

Once the hazard severity is characterized, the next step is to estimate the frequency or probability of the event. The frequency is a measure of the number of occurrences of a repeating event per unit time. The reciprocal of the return period (frequency) is the exceedance probability of the event, that is, the probability that the event is equaled or exceeded in any one year. For example, the 50-year flood has a probability of 0.02 or 2%, of being equaled or exceeded in any single year. There are a variety of methods for estimating the tsunami occurrence frequency including field observations, the study of historical records or by applying numerical models. Historical records of past events were analyzed in order to determine the frequency of a tsunami at the Alexandria site. Since tsunamis occur very rarely in a specific area, the estimation of their probability is a very difficult task with a high uncertainty in the results. Table 4 provides an example of the assessment of the annual probability (frequency) that is used in landslide risk assessment in Australia. This table helps us to interpret the estimated probability in our test sites as discussed in the following section.

**Table 4: Relation between verbal descriptor and indicative value of probability, source AGS, 2007**

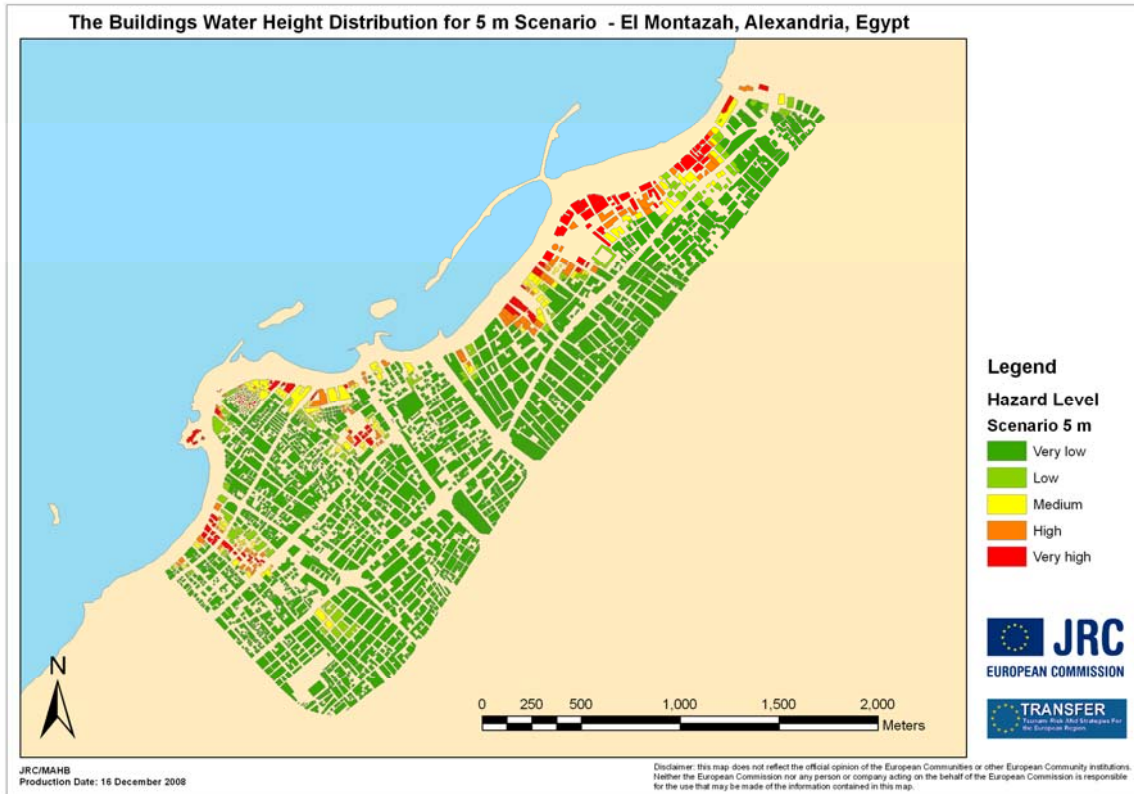
| Descriptor      | Indicative value | Recurrence interval |
|-----------------|------------------|---------------------|
| Almost certain  | $10^{-1}$        | 10 years            |
| Likely          | $10^{-2}$        | 100 years           |
| Possible        | $10^{-3}$        | 1000 years          |
| Unlikely        | $10^{-4}$        | 10 000 years        |
| Rare            | $10^{-5}$        | 100 000 years       |
| Barely credible | $10^{-6}$        | 1 000 000 years     |

### **3.2. Results of the Analysis**

In order to perform tsunami vulnerability and risk analysis, it is first necessary to select possible scenarios for future tsunami events. This is usually done based on historical data from past tsunamis or numerical modeling of tsunami propagation and inundation. Hamouda (2006) applied a numerical simulation with simple source models to examine a probable tsunami originating from the Hellenic Arc ridge of the Eastern Mediterranean. The maximum computed run-up height of about 9 m was found in Alexandria on the Egyptian Coast. The minimum estimated run-up height of about 2 m was found on the Western Egyptian Coast. El-Sayed, et al. (2000) used recent seismic activity, tsunami and ground motion modeling to infer the parameters of the possible sources previously proposed in the literature to discuss possible tsunami wave scenarios. Different magnitudes, focal mechanisms and depths were applied. The most probable modeling constellations complying with the reported damage for Alexandria resulted in tsunami wave heights ranging between 0.5 m and 5.8 m. On the basis of these two research studies two scenarios, a “medium” scenario of a 5 m run-up and a “worst-case” scenario of a 9 m run-up were defined in order to perform the physical vulnerability and risk analysis. For the two selected scenarios, the water height recorded at each building was used to characterize the tsunami hazard. Two so-called “flood hazard maps” or “building water distribution maps” were generated as a function of the water height for both areas, as illustrated in Figures 4a and 4b.



a)



b)

**Figure 4: The building water height distribution maps for the 5 and 9 m scenario in: a) El Gomrok area and b) El Montazah area, Alexandria**

The most affected buildings in the 5 m run-up height scenario are located in the north-western part of the El Gomrok area and along the coast in the El Montazah area. The maximum water height recorded for the 5 m scenario was about 4.0 m in both areas. As can be seen from the last picture showing the El Montazah area for the 9 m scenario, only the very high hazard level is presented because these building are located in a flat area of low elevation. The water height for this scenario ranged from 3.0 to 7.5 m, with a mean of 4.1 m.

In the next step, we have attempted to estimate the probability of the selected scenarios. The earthquakes occurring in the Hellenic arc-trench system are the main factors that generate tsunamis at the Egyptian coasts. During the years 365-1965, 38 earthquake events occurred in the Hellenic arc and were felt strongly in Egypt (El-Sayed et al. 2000). Within this long time period, extensive damage in Alexandria was reported only for two strong tsunamigenic earthquakes, which happened on 21 July 365 and 8 August 1303, respectively. These two events are also reported in the updated tsunami catalogues for the region of the Mediterranean Sea (Papadopoulus and Fokaefs, 2005) or in the National Geophysical Data Center (NGDC) maintained by the NOAA ([www.ngdc.noaa.gov](http://www.ngdc.noaa.gov)). The information present in historic records allowed a rough estimation of the tsunami frequency of 1/800 years, which corresponds to an indicative annual occurrence probability of  $1.25 \times 10^{-3}$ . According to Table 4, an event with such as low probability can “possibly” happen.

## 4. VULNERABILITY ANALYSIS

### 4.1. Introduction

The vulnerability to a tsunami is a function of a number of physical as well as social parameters that include amongst others: distance from the shore, depth of flood water, construction standards of buildings, preparedness activities, socio-economic status and means, level of understanding and hazard perception and amount of warning and ability to move away from the flood zone. Thus, a tsunami vulnerability analysis should be developed that includes as many of these factors as possible in order to gain a more realistic picture of spatial and temporal patterns of physical and social vulnerability (Papathoma et al., 2003).

Recently the need for 3D data describing built-up areas has increased. The availability of commercial very high resolution (VHR) optical satellite sensors such as IKONOS and QuickBird offer the possibility of stereo satellite data acquisition. Besides obtaining very detailed and up-to-date imagery of an area they allow the extraction of the third dimension and thus the generation of digital surface models (DSMs). DSMs can be used to extract information about the present built-up structures and affected population and be of great use in disaster management, damage, vulnerability and risk assessment analysis or urban planning.

Diverse research has been done dealing with height information extraction from stereo VHR satellite data since their availability. The research focused on different specific tasks such as on the development of physical models for improved orthorectification, or on DSM generation and the improvement of their accuracy (Eisenbeiss, et al., 2004, Toutin, 2001) with the focus on the ground control point distribution.

In order to derive a number of parameters describing physical vulnerability a digital surface model and a digital elevation model (DEM) were generated and consequently the building height derived. The information layers have been integrated in a GIS together with other geographical information layers (building outlines, coastline, etc.) and an integrative physical vulnerability analysis was performed. The vulnerability analysis in this study is composed of two parts, field data collection and satellite data processing which are discussed in the following sections.

## **4.2. Field Data Collection**

Four days field data collection was carried out in order to provide the following information about the building type and their main use:

- differential GPS points
- building type data for the two study sites
- structure type
- building height
- number of floors
- building function

In order to extract accurate orthorectified digital surface models from stereo data, precise ground control points (GCP) are required. The GCPs were collected using a Trimble GeoXT receiver. The data was differentially corrected by postprocessing. The reference base station was located in Alexandria. In total 21 GPS points were collected. Additionally, the GPS points served as validation for the horizontal and vertical accuracy of the orthorectified satellite scene and the derived heights of the DEM.

Building information was collected by GPS-based photography and laser altimeter which was then integrated in a GIS. In total 60 samples were collected, as illustrated in Figure 5. The buildings were selected randomly in the two study sites since a regular grid sampling was not feasible due to time constraints.



**Figure 5: Overview of the building type data collected in the two study sites (green stars)**

The building structure type was classified using the classification of the world housing encyclopedia (<http://www.world-housing.net>). In the study site areas only two classes were identified: reinforced concrete frame buildings and the buildings built following traditional standards using local expertise and material such as mortar, adobe and bricks. In El Gomrok, particularly in the old part of the district, older buildings are present, some of them in a neglected state, whereas in El Montazah buildings are more modern, taller and of higher standards. Examples of different types of buildings in the two districts of Alexandria are shown in Figure 6.



**Figure 6: Building types found in El Gomrok and El Montazah. Examples for a neglected building (upper left), a traditional brick building (upper right), a well maintained old building along the Corniche (lower left), a modern, tall building in El Montazah (lower right).**

### 4.3. Satellite Data, Processing and Resulting Products

For the study VHR IKONOS data was purchased. The data has a geometric resolution of 1 m (pan) and 4 m (multispectral) respectively. The stereo IKONOS dataset of Alexandria was acquired on 30th September 2007. The acquisition angles (Table 5) result in a base-to-height ratio of 0.58 which is considered good for the generation of a digital surface model.

**Table 5: Acquisition angles of the stereo IKONOS dataset**

|                            | Left image | Right image |
|----------------------------|------------|-------------|
| collection azimuth angle   | 171.0244   | 33.1512     |
| collection elevation angle | 73.88940   | 73.45229    |

The stereo satellite scenes were orthorectified using a) the attached rational polynomial coefficients (RPC) and b) using the RPCs and the measured GCPs. An overlap analysis of the four orthorectified scenes and the generated DSM showed that the RPC-based orthorectified left stereo scene matched best with the derived DSM and was consequently used for pansharpening. The pansharpened image was integrated in the GIS and served as information data layer in the vulnerability study.



**Figure 7: Quicklook of the acquired IKONOS stereo dataset**

For the DSM generation a non-commercial software package, named RSG was used. With the RSG software the stereo IKONOS scenes were map projected using the rational polynomials provided by the data provider and then optimized using linear add-on polynomials being determined from 9 collected GCPs. RMS, minimum and maximum values of point residuals, resulting from a backward transformation of control points into the image were used to conclude on the accuracy of the rational polynomial optimization (Table 6).

**Table 6: Point residual statistics achieved after rational polynomial optimization**

| Stereo Model | Res- X | Res-Y | Res-Z | Res-3D |
|--------------|--------|-------|-------|--------|
| RMS          | 1.30   | 1.28  | 2.13  | 2.80   |
| Min          | -2.58  | -1.96 | -3.74 | 1.39   |
| Max          | 1.75   | 2.24  | 3.02  | 4.66   |

For matching of the stereo scenes RSG uses an extended version of the “feature vector” matching method. It was developed at Joanneum Research, Institute of Digital Image Processing, Graz (Paar and Pölzleitner, 1992; Caballo-Perucha, 2003). The components of the “feature vectors” are in general represented by various convolution and variance filters or other suchlike features (selected featureset: Hfvm\_ikonos/H13, parameterset: Hfvm\_L6\_S4\_B3\_I100\_V1) (Raggam et al., 2005). Several parameters can be adjusted for the matching step such as the search window size (60l x 20p), the number of pyramids as well as the maximum back-matching distance (2.50). One essential feature is the cross correlation coefficient, which formerly used to be applied for image matching as such. Back-matching is used in order to get a reliability feed back for the individual matching results. Based on the results of the image matching, the digital raster surface model is then generated. It is achieved via 3D point intersection of the projected rays defined by the matched image points. In this step unreliable matching results, which will lead to wrong ground coordinates can be rejected. Subsequently, a regular raster surface model is interpolated. The gaps which may still be inherent to this raster model due to unreliable point rejection were interpolated using a versatile interpolation mechanism (Raggam et al., 2005). The resulting DSM is presented in Figure 8.

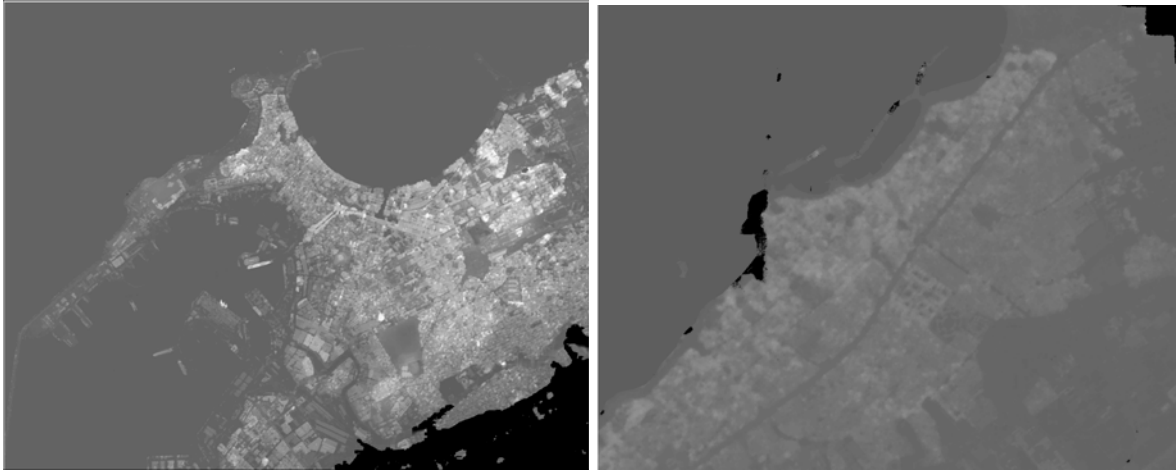


**Figure 8: Generated DSM for the two study sites, black areas represent no data areas or failed matching areas**

In order to know the height of an object the difference between a DSM and a DEM has to be known. This height difference was extracted in a semi-automatic way in 4 steps:

- 1) Erosion of object heights by application of morphological filter
- 2) Conversion of raster file into contour vector file
- 3) Manual editing of remaining object contours
- 4) Conversion and interpolation of edited contour vector file into raster file

The final DEM for the two study sites is illustrated in Figure 9.

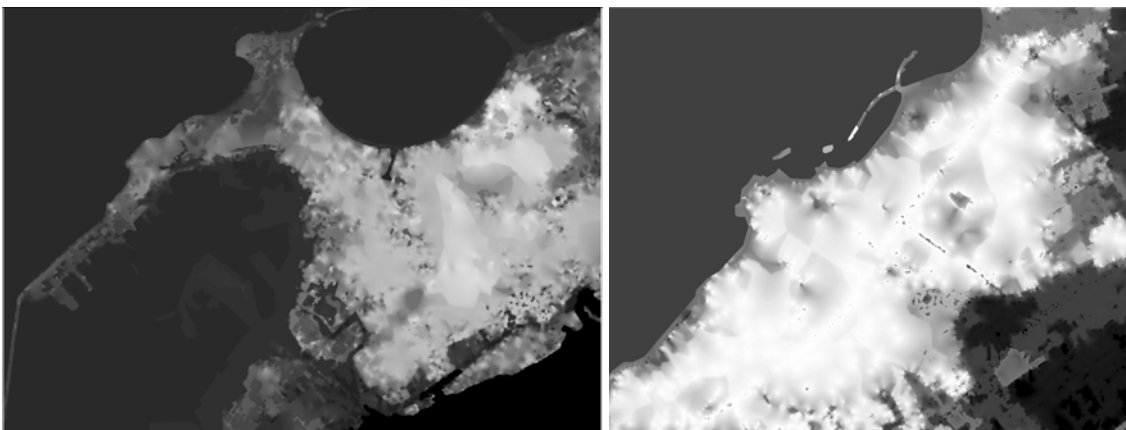


**Figure 9: Derived DEM for both study sites**

In a next step the DEM was subtracted from the DSM resulting in a building height layer. These layers were integrated in the GIS and for every building or building block polygon a medium elevation, building height and number of floors were calculated.

These layers were validated by comparing them with the collected GPS points and building data. Then root mean square error (RMSE) as well as mean absolute error (MAE) was calculated. An overview of the validation results is given in Table 7.

**Table 7: Accuracy assessment of the derived DEM, building height and number of floors layer**

| Data Layer      | No. of Samples | RMSE [m] | MAE [m] | MIN [m] | MAX [m] |
|-----------------|----------------|----------|---------|---------|---------|
| DEM El Gomrok   | 7              | 2.07     | 1.61    | -1.81   | 4.33    |
| DEM El Montazah | 6              | 2.46     | 2.22    | -3.24   | 3.18    |
| Building Height | 35             | 6.68     | 5.77    | -11.15  | 17.4    |
| No. of Floors   | 32             | 2.48*    | 2.02*   | -3.70   | 3.60*   |

\* indicates number of floors but not meters

It can be seen that the accuracy of the calculated DEMs range between 1.61 m and 2.46 m depending on the accuracy measure. This error might be slightly higher in the interpolated areas.

For the calculation of building height the DEM was subtracted from the initially generated DSM. The vertical accuracy of a DSM generated from stereo IKONOS data has proven to be around 3 m (RMSE) over built-up and impervious areas in the city of Graz, Austria (Eckert, 2008), which corresponds to approximately one floor. For cities consisting of many high-rise buildings, such as Alexandria this error is expected to be higher. High-rise buildings of 50 m are generally underestimated. A sample building of 94 m was underestimated by 65 m but it was excluded from the statistical accuracy analysis for statistical reasons. In El Gomrok only two business high-rise buildings are present. In El Montazah tall residential buildings are more common. Their height ranges usually between 40 m and 65 m. Exceptions are two luxury hotels present along the shore of El Montazah.

The calculated number of floors was determined with an accuracy of 2.48 (RMSE) or 2.02 (MAE) floors. Since the majority of the buildings in both study sites in Alexandria consist of at least 4 floors the error of 2 floors seems acceptable to use the information layer for physical vulnerability calculation.

#### 4.4. Vulnerability Parameters Derived from Generated Remote Sensing Products

The generated DSM and DEM offer a large variety of information layers to be calculated if a building/building block data layer is available. The average building height and number of floors can be calculated, among others. In this study the following parameters were directly or indirectly derived from the DSM or DEM:

- Average elevation at building centroid
- Average building height
- Number of floors
- Water height at every building for a 5 m and 9 m water level scenario

For the calculation of the physical vulnerability for every building/building block the four parameters listed in Table 8 were used.

**Table 8: Selected parameters for the physical vulnerability calculation and class allocation scheme**

| Parameter              | Vulnerability Class |         |            | Reference                   |
|------------------------|---------------------|---------|------------|-----------------------------|
|                        | low                 | medium  | high       |                             |
| Elevation [m]          | $\geq 10$           | 5-10    | $< 5$      |                             |
| Building type          | 2                   |         | 3          | Sandoval and Ferreras, 1991 |
| Number of Floors       | 5-21                | 3-4     | $< 3$      |                             |
| Shoreline Distance [m] | $> 400$             | 200-400 | $\leq 200$ | Ruangrassamee et al. 2006   |

Every parameter was weighted equally since the individual importance of each parameter and its influence for the two study sites in Alexandria is not known in detail. Every parameter was classified into three vulnerability categories and assigned a value. Depending on the sum of all values the building/building blocks were classified into the final physical vulnerability classification scheme of three and five classes. A selection of parameters for the study site El Gomrok is illustrated in Figures 10 – 12.



**Figure 10: Average elevation at every building polygon centroid**



**Figure 11: Calculated number of floors for every building polygon**

Additionally, the building data information collected in Alexandria was integrated in a GIS database by assigning the building structure/type and the building use to each building/building block. At last the distance from shore was calculated for every building/building block.



**Figure 12: Building type layer collected by visual examination in Alexandria**

#### **4.5. Physical Vulnerability Results**

The analysis of the physical vulnerability of buildings was performed for the same 5 m and the 9 m run-up scenarios as used for the tsunami hazard analysis. The resulting physical vulnerability maps in the two areas of the city of Alexandria are illustrated in Figure 13 and Figure 14.

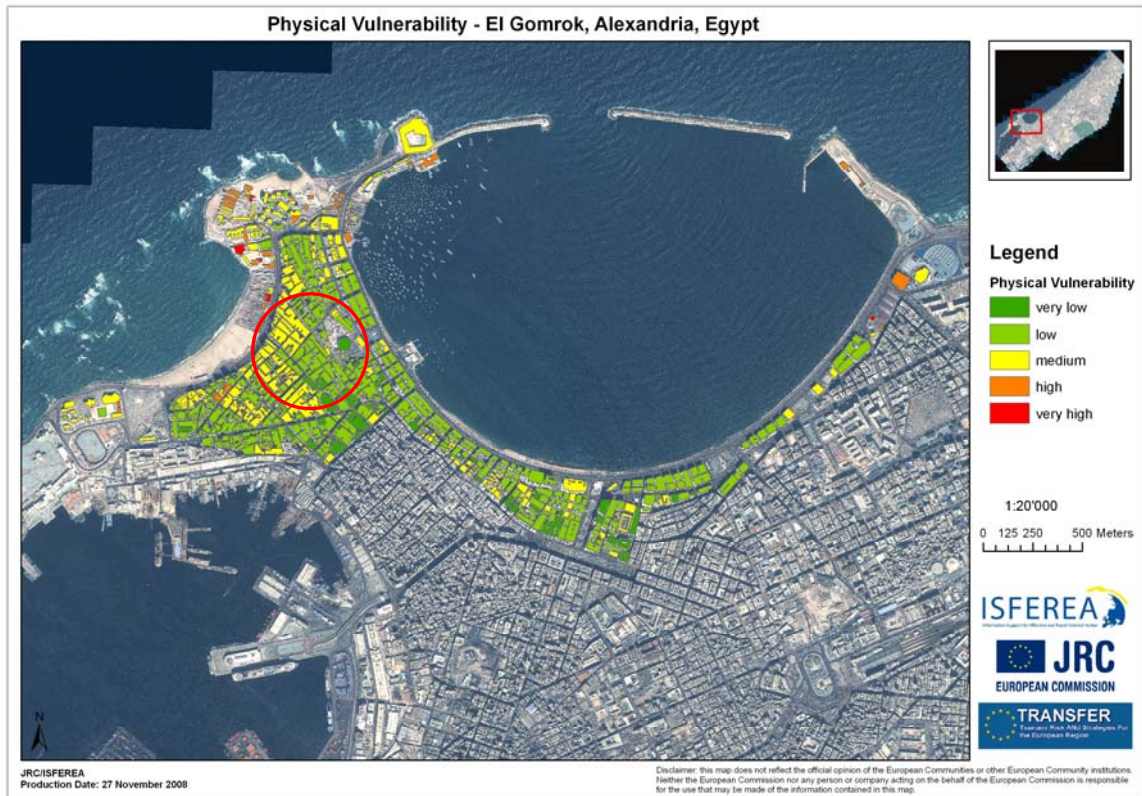


**Figure 13: Physical vulnerability map for the study site El Gomrok**

The resulting physical vulnerability map identifies the most vulnerable areas of El Gomrok along the shoreline in the north-west and north-east, where the urban areas are not protected by the harbor. In particular the urban area in the north-west (red circle) is most vulnerable to a tsunami. It is situated close to the shoreline and at a low elevation. Some of the built structures are old and not very high except for the front row towards the sea where some high-rise residential buildings of higher standard are present. In the north-east of El Gomrok buildings are vulnerable due to their short distance towards the open sea and the low elevation of the area.

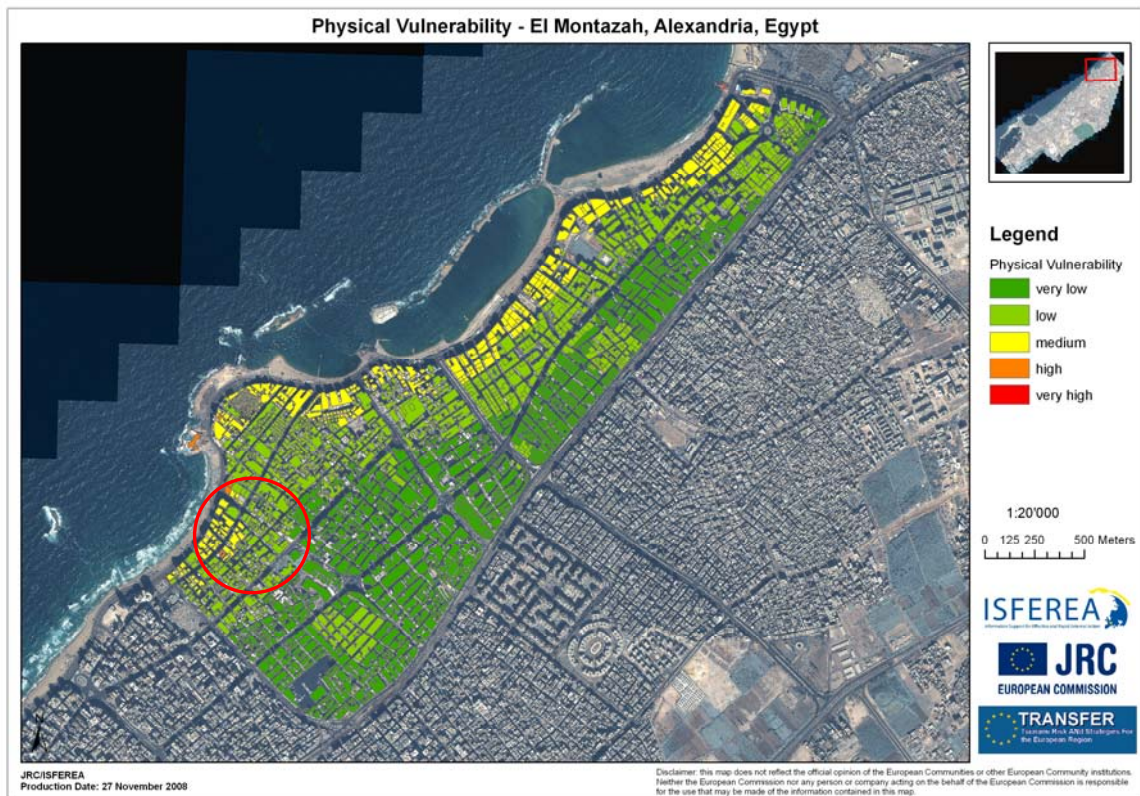


**Figure 14: Physical vulnerability map for study site El Montazah**

In the case of El Montazah the shoreline distance and elevation has the biggest influence on the physical vulnerability of the area. Most buildings are tall and of modern standards. Generally it can be said that the closer to the shore the more vulnerable the area, especially where no coastal barriers are present (red circle).

## 5. RISK ANALYSIS

### 5.1. Methodological Background

The term risk can have a different meaning in different applications or languages therefore it is necessary to clarify some basic definitions related to risk. In our understanding, the risk is the product of the likelihood that an undesired event such as a tsunami will happen within a specific period of time, and its consequences. In order to measure risk, it is necessary to define its characteristics, which are described in the process of risk analysis<sup>3</sup>. Tsunami risk analysis is a very complex process which requires knowledge of the tsunami

<sup>3</sup> Risk analysis is described as systematic use of information to identify sources and to estimate the risk. Risk analysis provides a basis for risk evaluation, risk treatment and risk acceptance.

source, the wave propagation and subsequent inundation, geographical conditions of the affected area, and social and economical aspects. The selected analysis approach therefore mainly depends on the data availability and quality. A more detailed description of tsunami risk assessment<sup>4</sup> is provided in a separate report (Jelínek and Krausmann, 2009) prepared by the JRC for the purposes of the TRANSFER project.

For the city of Alexandria we use the general UNDP (2004) definition of risk as the product of a hazard and its consequences. The consequence analysis includes the identification of the elements at risk (e.g. population, building, economic activities, infrastructures, and environment) and the determination of the vulnerability of the selected elements (e.g. persons or property). In mathematical form, the following general expression can be used:

$$R = H \times V$$

where, R = risk, H = probability of tsunami hazard occurrence, and V = vulnerability of the elements at risk.

Risk usually refers to population, built structures or the natural environment. In this study, we estimate tsunami risk for structures, or the built environment. We did not estimate the risk to the population as the required data was not available at the time we performed our study. The tsunami risk to physical property was estimated in a qualitative way using a ranking risk matrix of 5 x 5 classes which relates hazard and vulnerability. The hazard levels were assigned according to Table 3, while the vulnerability scores are based on Table 8. The scores for hazard and vulnerability were multiplied, and a final score from 1 to 25 was then assigned to the different risk categories, as illustrated in Table 9.

The results of the tsunami risk matrix are 5 risk levels. For the very low risk level, both the hazard category and the vulnerability are very low while for the very high risk, at least one category of the hazard or vulnerability must be high or very high and the second at least high. Indeed, the determination of this level rating is very subjective. In the final step of the

---

<sup>4</sup> Risk assessment is an overall process of risk analysis and risk evaluation.

analysis the risk matrix is translated into thematic risk zonation maps in a GIS environment.

**Table 9: Tsunami risk level matrix**

| Vulnerability | Hazard          |                 |                 |                  |                  |
|---------------|-----------------|-----------------|-----------------|------------------|------------------|
|               | VL (1)          | L (2)           | M (3)           | H (4)            | VH (5)           |
| VL (1)        | VL<br>1 x 1 = 1 | L<br>1 x 2 = 2  | L<br>1 x 3 = 3  | L<br>1 x 4 = 4   | M<br>1 x 5 = 5   |
| L (2)         | L<br>2 x 1 = 2  | L<br>2 x 2 = 4  | M<br>2 x 3 = 6  | M<br>2 x 4 = 8   | H<br>2 x 5 = 10  |
| M (3)         | L<br>3 x 1 = 3  | M<br>3 x 2 = 6  | M<br>3 x 3 = 9  | H<br>3 x 4 = 12  | H<br>3 x 5 = 15  |
| H (4)         | L<br>4 x 1 = 4  | M<br>4 x 2 = 8  | H<br>4 x 3 = 12 | H<br>4 x 4 = 16  | VH<br>4 x 5 = 20 |
| VH (5)        | M<br>5 x 1 = 5  | H<br>5 x 2 = 10 | H<br>5 x 3 = 15 | VH<br>5 x 4 = 20 | VH<br>5 x 5 = 25 |

Risk range: Very Low (=1); Low (2-4); Medium (5-9); High (10-16); Very High (17-25)

## 5.2. Tsunami Risk Results

The tsunami risk analysis was conducted by combining the estimated tsunami hazard and physical vulnerability using the risk matrix illustrated in Table 9. The results of the tsunami risk analysis carried out for the 5 m and 9 m scenarios in the two selected regions are illustrated in Figures 15 to 18.



a)



b)

**Figure 15: Tsunami building risk zonation maps in the El Gomrok area for: a) 5 m scenario and b) 9 m scenario**

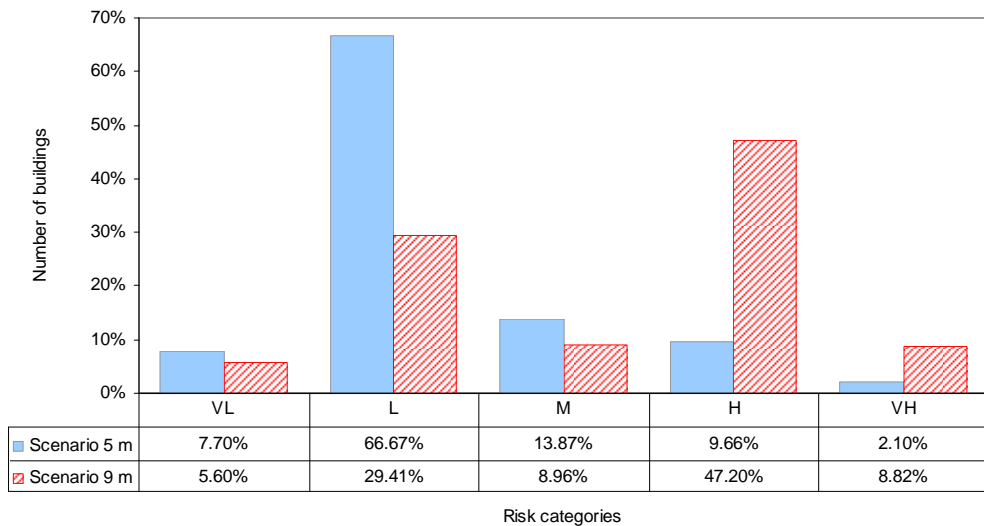
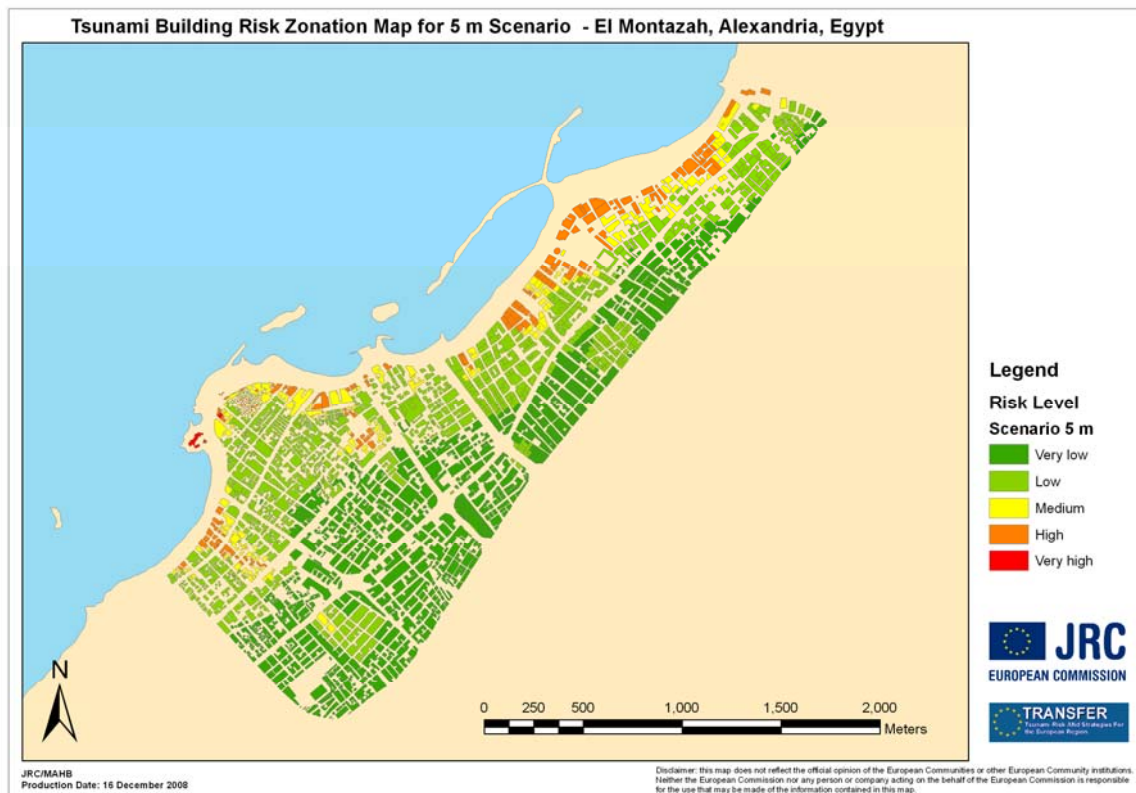


**Figure 16: Pair column chart of tsunami building risk for the 5 m event (in blue) and the 9 m scenario (red stripes)**

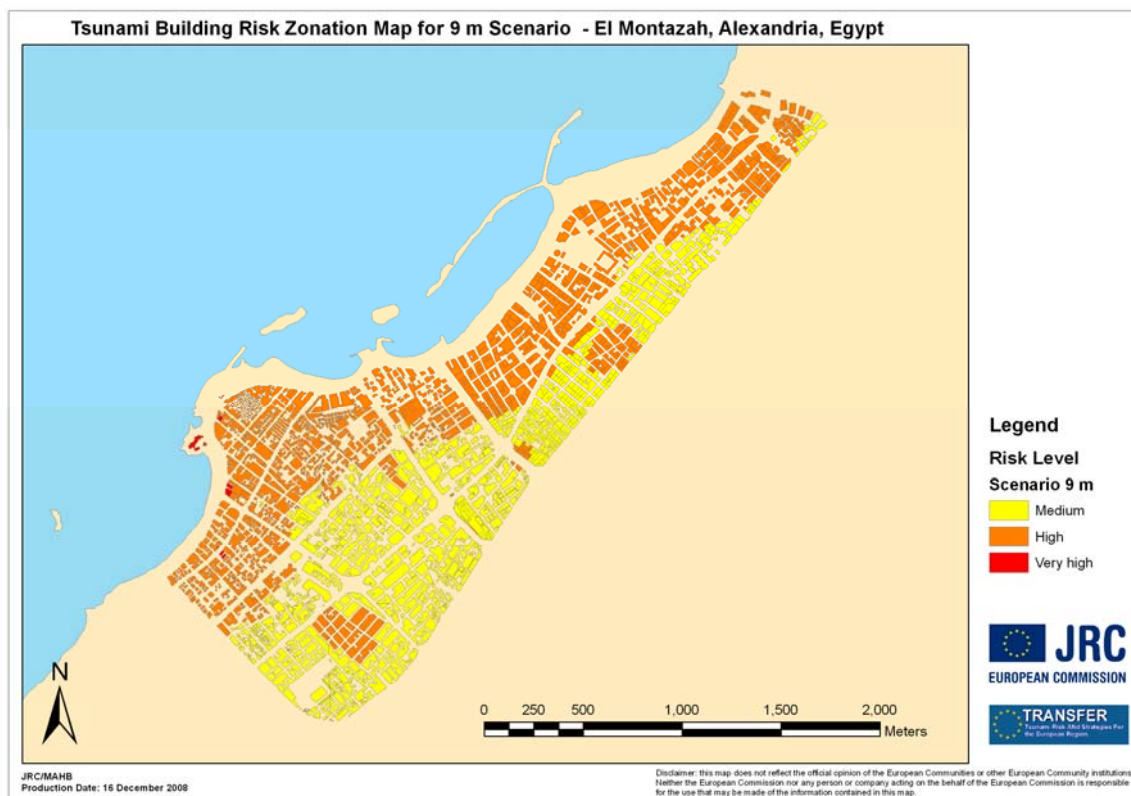
The tsunami building risk zonation map (Figure 15) and the corresponding chart (Figure 16) indicate that 11.76 % of the buildings in El Gomrok are at high or very high risk for the

5 m scenario, while the same applies to 56.02 % for the 9 m scenario. The majority of these buildings are located in the north-west and partly in the north-east part of the studied area.

For the 5 m scenario in the El Montazah area the level of risk to buildings is low (Figure 17). This is in contrast with the results of the 9 m scenario, where the majority of the buildings are in the high or very high risk level. These buildings are usually located along the coast. This is better illustrated in the direct comparison between the two scenarios in Figure 18, which shows how the building risk level for the same area changes as a function of the selected scenario. There are no buildings located in the very low or the low risk level for the 9 m scenario.



a)



b)

**Figure 17: Tsunami building risk zonation maps in El Montazah area for: a) 5 m scenario and b) 9 m scenario**

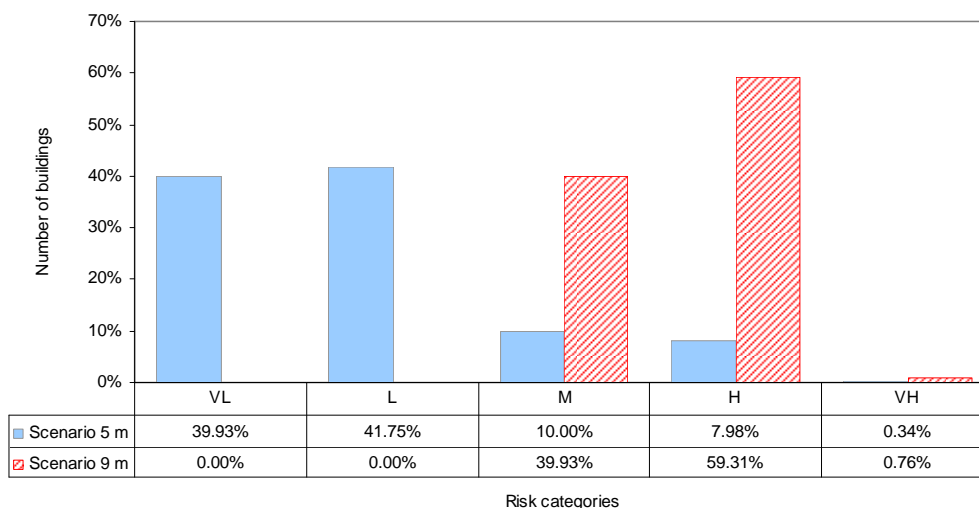


**Figure 18: Chart showing distribution of tsunami risk in El Montazah area for 5 (in blue) and 9 m (red stripes) scenarios**

In the next step of our risk analysis we focused only on the most dangerous areas, which were the buildings located in the very high and high risk levels. The resultant tsunami

building risk zonation maps were combined with the building-use database prepared during the field trip. As a result we obtained a distribution of the selected building types for the two scenarios in both areas, as summarized in Table 10.

**Table 10: Distribution of building types in the investigated areas**

| El Gomrok, (5 m/9 m scenario) |            |          |          |          |              |           |               | El Montazah, (5 m/9 m scenario) |       |          |        |              |           |                 |
|-------------------------------|------------|----------|----------|----------|--------------|-----------|---------------|---------------------------------|-------|----------|--------|--------------|-----------|-----------------|
| Risk level                    | Resid/comm | Military | Industry | Commerce | Governmental | Religious | Total         | Resid/comm                      | Hotel | Hospital | School | Governmental | Religious | Total           |
| VH                            | 2/16       | 8/10     | 1/31     | 4/6      | 0/0          | 0/0       | <b>15/63</b>  | 8/18                            | -     | -        | -      | -            | -         | <b>8/18</b>     |
| H                             | 42/270     | 4/11     | 14/43    | 8/6      | 1/2          | 0/5       | <b>69/337</b> | 183/1391                        | 5/5   | 0/2      | 0/5    | 0/1          | 1/1       | <b>189/1405</b> |

VH- very high, H- high

It can be seen that most buildings belong to the residential or industrial type in both investigated areas. Special attention must be paid to the residential buildings, where we can expect a high population density. The number and distribution of hospitals, as well as their capacity can influence the physical vulnerability. Unfortunately, precise data on the building use were not available and could not be collected during our short field visit. It is, however, of vital importance that disaster managers and emergency planners have detailed information on which buildings, infrastructural units and groups of people are particularly vulnerable to tsunami impacts. When such data is available, cost effective mitigation measures may be developed and applied.

## 6. DISCUSSION AND CONCLUSIONS

Tsunami building vulnerability and risk maps were prepared for two selected scenarios of 5 m and 9 m run-up height in two districts of the city of Alexandria. These maps can help the relevant authorities to effectively prepare, mitigate and manage this hazard. Implementation of appropriate risk reduction measures should be particularly taken into consideration in the “very high” and “high” risk level areas.

## **Hazard Analysis**

Tsunami building water height distribution maps were generated to characterize the tsunami hazard in Alexandria. These maps were prepared based on the water height recorded at each building using a bathtub approach. According to our experience gained in this study, the bathtub approach can be recommended for a preliminary analysis to identify hot spots areas of tsunami risk. In the future, additional parameters can be included to characterize the tsunami hazard, such as wave height, current velocity, tsunami intensity or magnitude. In this case, numerical modeling of the tsunami wave propagation and inundation must be employed. The water height map for the 9 m scenario showed that the water covers all of the buildings in the El Montazah district. Therefore, a different, more detailed hazard classification can be considered for futures studies.

The determination of the frequency of a future tsunami was not an easy task due the limited number of data on historical events. If detailed historical information about past events with corresponding run-up will become available, it will be possible to assign a more precise probability to a specific scenario.

## **Vulnerability Analysis**

Data from different sources were used to analyze risk in a GIS environment. Remote sensing can provide an effective and updated data source for physical vulnerability and risk analysis. Several parameters were derived independently from the stereo dataset, such as elevation, building height and number of floors. In addition, the building type and main use were obtained from the field survey. The distance from the shoreline generally shows decreasing vulnerability and therefore risk but the combination with elevation, building height and building type may lead to a different pattern.

In this study every parameter contributing to the physical vulnerability was equally weighted since individual weighting of each parameter requires an in-depth knowledge of a tsunami scenario and its impact on an area which is not available for Alexandria.

## **Risk Analysis**

Two tsunami building risk zonation maps for each studied area in the city of Alexandria were prepared using a combination of the calculated hazard information and the building vulnerability. The main concern of the risk analysis performed in this study was to identify

high and very high tsunami building risk areas in order to help local authorities to concentrate their attention to these areas. In particular, the tsunami risk for the 9 m scenario showed that more than 50 % of the buildings are located in the very high risk zones. An analysis of the building use showed that the majority of these buildings are residential or industrial types, highlighting that the potential consequences of a tsunami could be severe.

Risk analysis is an uncertain science and this uncertainty affects all specific components of risk analysis. It is therefore evident that the accuracy of the resultant risk maps is highly dependent on the accuracy of its individual components (hazard and vulnerability). The tsunami hazard is characterized by a wide range of variation regarding tsunamigenic sources, magnitude and frequency of the event. A high uncertainty is also associated with the estimation of vulnerability and its indicators. The errors are propagated and consequently a high uncertainty in the final tsunami risk results is likely.

### **Tsunami risk reduction**

There are a variety of measures that could be used to reduce the consequences of a tsunami. In general they can be divided into two groups: structural and non-structural. Structural measures can reduce risk e.g. by using engineering solutions such as reinforcing or strengthening of the buildings that may be damaged or cause injury; coastal protection of the area using for example tsunami defense structures or reduction of the impact of tsunami wave prior to reaching the shoreline (e.g. break waters). Non-structural mitigation includes providing people with basic information on tsunami risk, education or training, because community awareness and preparedness are the most important factors to reduce potential losses due to tsunami. The structural mitigation measures for the city of Alexandria should particularly focus on the buildings located in the very high and high risk levels. The city of Alexandria is highly populated, therefore the development of an effective emergency evacuation plan, if not already existing, is highly recommended. Another mitigation measure is the implementation of a warning system that should also be considered for the Alexandria site. In addition, the preparation of a detailed inventory of the critical facilities located in the potential inundation areas would be very useful.

## REFERENCES

AGS 2007: Guideline for landslide susceptibility, hazard and risk zoning for land use planning. Australian Geomechanics Society, Australian Geomechanics 42:1

Alexander, D. 2000: Confronting Catastrophe, Terra Publishing, 282 pp

Boschi, E., Tinti, S., Armigliato, A., Graziani, L., Manucci, A., Maramai, A., Mazza, S., Pagnoni, G., Tonini, R., Zaniboni, F. 2005: A tsunami warning system for the Mediterranean: an utopia that could be implemented in a short time. Geophysical Research Abstracts, Vol. 7, 09852, SRef-ID: 1607-7962/gra/EGU05-A-09852

Caballo-Perucha, M. 2003: Development and analysis of algorithm for the optimization of automatic image correlation. M.S. thesis, Post-graduate University Course Space Science, Karl-Franzens-Universität Graz, Austria.

Curtis, G.D. and Pelinovsky, E.N. 1999: Evaluation of tsunami risk for mitigation and warning, Science of Tsunami Hazards 17/3: 187-192

Eckert, S. 2008: 3D-Building height extraction from stereo IKONOS data, EU report, ISBN-978-92-79-05127-2, 60 pp

Eckert, S. and Zeug, G. 2009: Assessing tsunami vulnerability in Alexandria, Egypt by using optical VHR satellite data, 33rd Int. Symp. Remote Sensing of Environment – Sustaining the Millennium Development Goals, Stresa, May 2009

Eisenbeiss, H., Baltsavias, E., Pateraki, M. and Zhang, L. 2004: Potential of IKONOS and QUICKBIRD imagery for accurate 3D point positioning, orthoimage and DSM generation. Proc. 20th ISPRS Congress, Istanbul, 2004, 522-528

El-Sayed, A., Romanelli, F. and Panza, G. 2000: Recent seismicity and realistic waveforms modeling to reduce the ambiguities about the 1303 seismic activity in Egypt, Tectonophysics 328: 341-357

Frihy, O.E. 2003: The Nile Delta – Alexandria Coast: Vulnerability to sea-level rise, consequences and adaptation. Mitigation and Adaptation Strategies for Global Change. 8: 115-138

Hamouda, A.Z. 2006: Numerical computations of 1303 tsunamigenic propagation towards Alexandria, Egyptian Coast. Journal of African Earth Sciences, 44: 37-44

Jelínek, R. and Krausmann, E. 2009: Approaches to tsunami risk assessment, EUR 23573 EN, JRC48713, Luxembourg (Luxembourg): OPOCE, 50 pp.

NGDC, National Geophysical Data Center, NOAA Satellite and Information Service, <http://www.ngdc.noaa.gov/hazard/hazards.shtml>

Paar, G. and Pölzleitner, W. 1992: Robust disparity estimation in terrain modelling for spacecraft navigation. Proc. 11th ICPR, International Association for Pattern Recognition, 738-741

- Papathoma, M., Dominey-Howes, D., Zong, Y. and Smith, D. 2003: Assessing tsunami vulnerability, an example from Herakleio, Crete. *Natural Hazards and Earth System Sciences*, 3: 377-389
- Papadopoulos, G.A. and Dermentzopoulos, Th. 1998: A Tsunami Risk Management Pilot Study in Heraklion, Crete, *Natural Hazards* 18: 91–118
- Papadopoulos, G., A. and Fokaefs, A. 2005: Strong tsunamis in the Mediterranean sea: A re-evaluation, *ISSET Journal of Earthquake Technology*: 463/42/2, 159-170
- PREVIEW, 2005: PREvention, Information and Early Warning preoperational services to support the management of risks, Damage assessment based on damage intensity scales: service specification. <http://www.preview-risk.com/>
- Raggam, H., Franke, M., Ofner, M. and Gutjahr, K. 2005: Accuracy assessment of vegetation height mapping using spaceborne IKONOS as well as aerial UltraCam stereo images. 25th EARSeL Symposium, Workshop on “3D Remote Sensing”, Porto, Portugal, Jun. 10-11.
- Ruangrassamee, A., Yanagisawa, H., Foytong, P., Lukkunaprasit, P, Koshimura, S. and Imamura, F. 2006: Investigation of tsunami-induced damage and fragility of buildings in Thailand after the December 2004 Indian Ocean tsunami. *Earthquake Spectra*, 22: 377-401
- Rynn, J. and Davidson, J. 1999: Contemporary assessment of tsunami risk and implication for early warnings for Australia and its island territories, *Science of Tsunamis Hazards*: 17/2, 107-125
- Sandoval, F.J. and Farreras, S. F. 1991: On tsunami resonance of the gulf of California. In: *Tsunamis in the World: Proceedings of the Fifteenth International Tsunami Symposium*, Vienna, Austria 1991
- Toutin, T. 2001: Elevation modelling from satellite visible and infrared (VIR) data. *International Journal of Remote Sensing*, 22: 1097-1125
- UNU-EHS, 2009: Vulnerability Assessment within Alexandria test site, Deliverable D 8.8 of TRANSFER project, 6<sup>th</sup> European Framework Programme.
- United Nations Development Programme (UNDP), 2004: Reducing disaster risk. A challenge for development. A Global Report, UNDP—Bureau for Crisis Prevention and Recovery (BRCP), New York.



European Commission

**EUR 23967 EN – Joint Research Centre – Institute for the Protection and Security of the Citizen**

Title: Tsunami Vulnerability and Risk Analysis Applied to the City of Alexandria, Egypt

Author(s): Róbert Jelínek, Sandra Eckert, Gunter Zeug, Elisabeth Krausmann

Luxembourg: Office for Official Publications of the European Communities

2009 – 40 pp. – 21 x 29.7 cm

EUR – Scientific and Technical Research series – ISSN 1018-5593

**Abstract**

This report describes the work carried out by two actions of the JRC, ISFEREA and MAHB, to achieve the TRANSFER project objectives, which was to produce tsunami risk-related products for the town of Alexandria. The deliverable D8.8 of the TRANSFER project specifies the production of flooding maps, vulnerability maps with selected indicators and scenario risk maps. The ISFEREA action performed the physical vulnerability assessment with a help of high resolution satellite remote sensing data and a field survey. The vulnerability was calculated based on four indicators such as the elevation, building type, number of floors and shoreline distance. The results of vulnerability assessment have been used for the purposes of risk analysis, which was done by the MAHB action. The tsunami risk was calculated in a qualitative way using a risk matrix relates the hazard and vulnerability.

The study was carried out in two districts, a central and peri-urban of the city of Alexandria. Two scenarios of a 5 m and a 9 m inundation were selected for the analysis based on historical records of past tsunamis. The information obtained in this study can help responsible authorities to reduce potential tsunami consequences based on the resultant tsunami building vulnerability and risk maps.



The mission of the JRC is to provide customer-driven scientific and technical support for the conception, development, implementation and monitoring of EU policies. As a service of the European Commission, the JRC functions as a reference centre of science and technology for the Union. Close to the policy-making process, it serves the common interest of the Member States, while being independent of special interests, whether private or national.

